

# The effect of twin boundaries on the spectroscopic performance of CdZnTe detectors

B.H. Parker\*<sup>a</sup>, C.M. Stahle<sup>a</sup>, D. Roth<sup>b</sup>, S. Babu<sup>a</sup>, J. Tueller<sup>a</sup>  
<sup>a</sup>NASA Goddard Space Flight Center; <sup>b</sup>NASA, Glenn Research Center

## ABSTRACT

Most single grains in cadmium zinc telluride (CdZnTe) grown by the high-pressure Bridgman (HPB) technique contain multiple twin boundaries. As a consequence, twin boundaries are one of the most common macroscopic material defects found in large area (400 to 700 mm<sup>2</sup>) CdZnTe specimens obtained from HPB ingots. Due to the prevalence of twin boundaries, understanding their effect on detector performance is key to the material selection process. Twin boundaries in several 2 mm thick large area specimens were first documented using infrared transmission imaging. These specimens were then fabricated into either 2 mm pixel or planar detectors in order to examine the effect of the twin boundaries on detector performance. Preliminary results show that twin boundaries, which are decorated with tellurium inclusions, produce a reduction in detector efficiency and a degradation in resolution. The extent of the degradation appears to be a function of the density of tellurium inclusions.

Keywords: CdZnTe, High Pressure Bridgman, twins, detectors

## 1. INTRODUCTION

CdZnTe detectors, which have the advantages of room temperature operation, high absorption efficiency and high resolution<sup>1,2</sup>, are being employed in hard x-ray and gamma ray astronomical missions such as the SWIFT Burst Alert Telescope (BAT)<sup>3</sup>, the International Focusing Optics Collaboration for  $\mu$ Crab Sensitivity (InFOC $\mu$ S)<sup>4</sup>, the Energetic X-ray Imaging Telescope Experiment (EXCITE)<sup>5</sup> and the High Energy Focusing Telescope (HEFT)<sup>6</sup>. CdZnTe detectors will also most likely be used on future high energy missions such as the Constellation X-ray Mission (Con-X) Hard X-ray Telescope (HXT)<sup>6</sup> and the Energetic X-ray Imaging Survey Telescope (EXIST)<sup>5</sup>. One of the challenges for most of these missions is obtaining large area (400 to 700 mm<sup>2</sup>) bulk CdZnTe specimens which are free of defects deleterious to detector performance.

In order to support these programs, the Materials Engineering Branch at NASA Goddard Space Flight Center has developed a process for mining large area specimens from HPB CdZnTe produced by eV Products, Inc. This mining process is based on the results of a correlation study between bulk material defects and detector performance.<sup>7</sup> The process has yielded numerous single grain large area (>700 mm<sup>2</sup>) bulk specimens, of which approximately 70 percent contain one or more twin boundaries. Previous work using a x-ray spectral mapping system indicated that twins in several of the mined specimens did not produce a detectable degradation in detector performance. This result was obtained with detectors configured with large anode pixels (12.5 by 12.5 mm) and a collimated, but relatively non-monochromatic x-ray source.

The contention within the CdZnTe community was that our inability to detect the twins was due to the large pixel size used for spectral mapping. The theory was that distortions in the electric field created by a twin would not show up in a large pixel device, as all the induced charge would still be collected. Whereas in a small pixel device, distortions in the electric field would produce charge channeling to adjacent pixels and result in an area of poorer performance. In this paper we describe our efforts to determine the effect of twins on detector performance and to gain insight into whether charge is channeled or trapped by twins.

---

\*Further author information: (Send correspondence to Bradford H. Parker)  
E-mail: bparker@mscmail.gsfc.nasa.gov

## 2. EXPERIMENT

### 2.1 Infrared Transmission Imaging

Our infrared transmission imaging setup, which utilizes an Inframetrics Model 760 radiometer operating in the 8 to 12 micron bandwidth, has been previously described in the literature.<sup>7</sup> Recently, we employed a face staining etch,<sup>8</sup> to establish that the linear features decorated with tellurium inclusions that we typically see in HPB CdZnTe are twin boundaries. Figure 1 shows an optical image of a 15 by 15 by 2 mm CdZnTe specimen after etching. The specimen clearly contains multiple twin boundaries. The radial lines in the image are remnants of cutting saw damage. The corresponding infrared transmission image which is

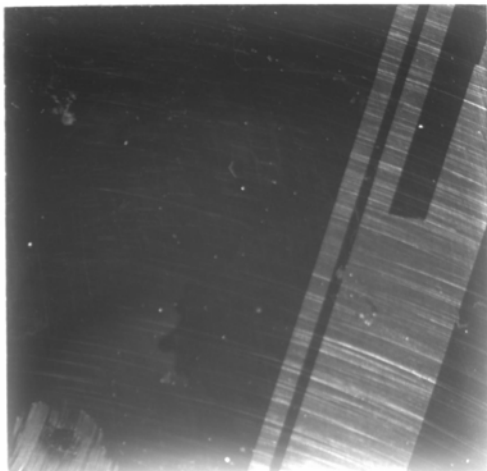


Figure 1. Optical photograph of a 15 by 15 by 2 mm HPB CdZnTe specimen after application of a face staining etch. The lighter areas correspond to twinned regions.

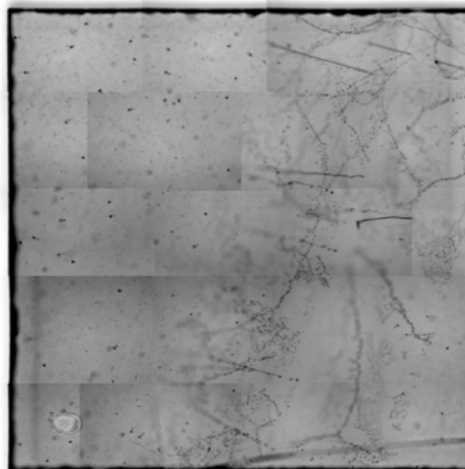


Figure 2. Infrared transmission image of the HPB CdZnTe specimen shown in Figure 1. The twin planes, which are at a relatively shallow angle, are decorated with strings of tellurium inclusions.

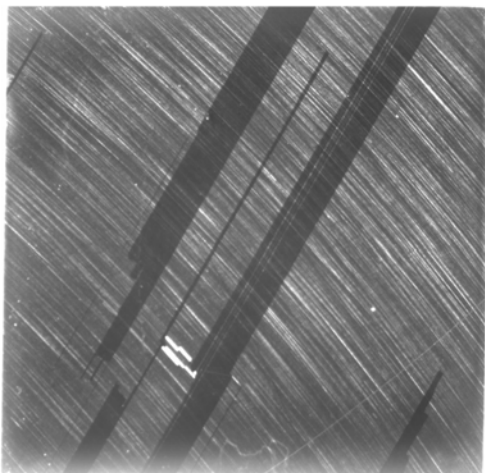


Figure 3. Optical photograph of a 15 by 15 by 2 mm HPB CdZnTe specimen after application of a face staining etch. The darker areas correspond to twinned regions.

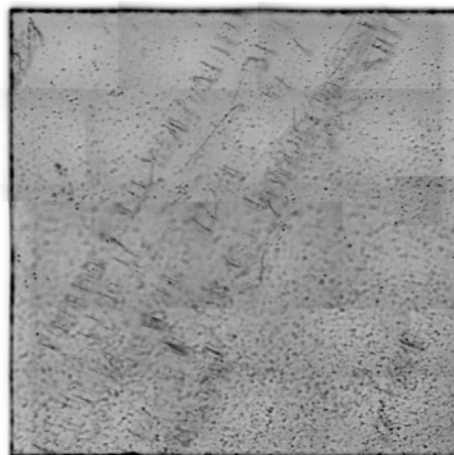


Figure 4. Infrared transmission image of the HPB CdZnTe specimen shown in Figure 3. The twin planes are at a relatively steep angle and decorated with tellurium inclusions.

shown in Figure 2, shows that the twins are decorated with tellurium inclusions. The inclusions often appear in strings which are confined to the plane of the boundary. Figures 3 and 4 show the correlation between the etch and the infrared transmission image for an additional 15 by 15 by 2 mm specimen.

To the best of our knowledge, all twins in HPB CdZnTe are decorated with tellurium inclusions. The density of the inclusions on the twin plane is significantly less than the density of the inclusions found on typical grain boundaries. However, in the areas where the inclusions appear as strings, the density of inclusions is greater than that seen in the surrounding material.

## 2.2 Detectors with 2 mm pixels

Several 26.9 by 26.9 by 2mm HPB CdZnTe specimens containing twins were fabricated into devices with a 12 by 12 grid of 2 mm anode pixels (2.1 mm pitch) and a planar cathode. Both the anode and cathode contacts were sputtered platinum applied by eV Products, Inc. In order to evaluate the uniformity of the pixel response, we employed a nine pin test fixture designed to contact a central pixel, which is being evaluated, as well as the surrounding eight pixels to insure a uniform electric field. The pixel response was measured using discrete electronics consisting of an eV Products, Inc. Model 550 preamplifier and a PC based APTEC Model 5004 MCA with an on-board amplifier. A bias voltage of +250 Volts was applied to all nine contacted pixels. We used Am<sup>241</sup> as a source of photons and the device was flood illuminated from the cathode side. A silver-loaded silicon (CHO-SEAL 1224) was used as an electrically conductive interface between the test fixture beryllium window and the device cathode. A vertically conductive sheet consisting of 30 micrometer diameter gold plated brass wires imbedded in symmetric rows and columns in a silicon rubber sheet (Shin-Etsu GB-Matrix) was used to make electrical contact between the nine pogo pins and the anode pixels. This setup was used to evaluate the response of 96 of the 144 pixels on a device. When the test fixture contacted an edge pixel (six of the nine pogo pins in contact with the device), the pressure produced by the spring loaded pogo pins and the compliance of the CHO-SEAL 1224 were both sufficient to cause the opposite side of the specimen to tilt upward. Hence, we were unable to reliably measure the response of the 44 edge pixels, as well as the four pixels adjacent to the corners. A spectrum was collected for each of the 96 central pixels and the position and FWHM of the Am<sup>241</sup> 59.6 keV line was measured and mapped.

## 2.3 X-ray spectral mapping

Our x-ray spectral mapping system has also been previously described in the literature.<sup>7</sup> In summary, a CdZnTe specimen is configured as either a planar or large pixel (10 mm or greater) detector. The same pulse height spectrum electronics described in the previous section are used for spectral acquisition. The biased detector is mounted on a motorized stage and moved relative to a collimated beam of x-rays from a 160 kV micro-focus x-ray tube. Scans typically employ either a 100 or 250 micrometer diameter tungsten collimator with a corresponding step size. The x-ray spectrum from the tube consists of characteristic x-ray lines from the tube anode (tungsten) superimposed on a continuous spectrum. The position and number of counts in the tungsten K-alpha line at 59.3 keV are typically mapped. Spectral acquisition and motion are controlled using LabView.<sup>TM</sup>

We have recently made several system improvements. First, in order to create a more monochromatic source of photons, we have employed a 200 micrometer thick tungsten filter. Now the amplitude of the characteristic tungsten lines in the collimated beam of photons is a combination of the anode output and the filter and collimator fluorescence. The tungsten filter has significantly reduced the low energy component of the spectrum and provides a k-edge filter (69.4 keV) at energies higher than the tungsten K-alpha (59.3 keV) and K-beta (67.3 keV) lines. The resultant peak-to-valley ratio for the 59.3 keV line is approximately 6 to 8 (the higher values are obtained when CHO-SEAL 1224 is employed, as the silver provides additional low energy filtering). Without the tungsten filter the ratio was 2 to 3. In Figure 5, a typical spectrum of the system as detected by a CdZnTe detector is shown in comparison to an Am<sup>241</sup> spectrum collected from the same detector. We have also made significant improvements in the LabView<sup>TM</sup> software used for data acquisition.<sup>9</sup> Most importantly, we now store the entire spectrum for each point in a scan. Previously, we only stored specific information, such as peak channel and peak channel counts, for each scan point.

Having the entire spectrum allows us to employ post data acquisition averaging to reduce noise and provides the ability to examine subtle features such as hole tailing.

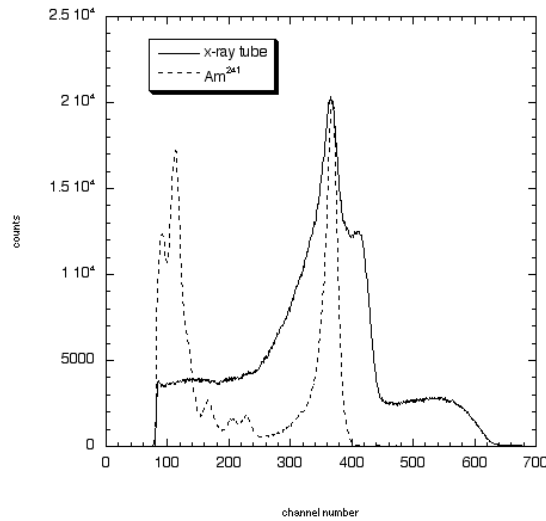


Figure 5. Typical spectrum from our 160 kV microfocus x-ray tube with a 200  $\mu\text{m}$  tungsten filter and 250  $\mu\text{m}$  tungsten collimator in place. For comparison, an uncollimated  $\text{Am}^{241}$  spectrum is shown.

### 3. RESULTS

#### 3.1 Detectors with 2 mm pixels

The 26.9 by 26.9 by 2 mm specimens evaluated in the 2 mm pixel configuration are single grain specimens which were mined from eV Products, Inc. HPB wafer slices in support of the InFOC $\mu$ S program. The first specimen contains three planar and parallel twin boundaries. The through-the-thickness angle and the lateral distance between the twin boundaries is shown schematically in Figure 6 and an infrared transmission image of the specimen is shown in Figure 7. The map of the peak channel position for the  $\text{Am}^{241}$  59.6 keV line, which is shown in Figure 8, has the same orientation as the infrared transmission image shown in Figure 7. The pixel map shows that the twin region produces a slight downward shift in the peak channel position. The scatter plot of peak channel position versus the FWHM for the 59.6 keV line, which is shown in Figure 9, shows that the downward shift in peak channel position is accompanied by a slight degradation in resolution. Because the twin planes traverse the specimen faces at an angle, there is considerable variability in the amount of pixel area intersected by the twin planes for any pixel designated as being on the twin. Likewise, as can be seen in Figure 7, the density of tellurium inclusions on the twin planes is also variable. These variations undoubtedly contribute to variations in the response for those pixels designated as being on the twin. Figure 10 shows the  $\text{Am}^{241}$  spectra for the most efficient pixel off the twin versus the least efficient pixel on the twin.

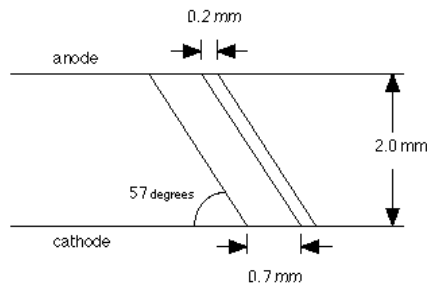


Figure 6. Schematic drawing of the three twin planes in the first 2mm pixel specimen.

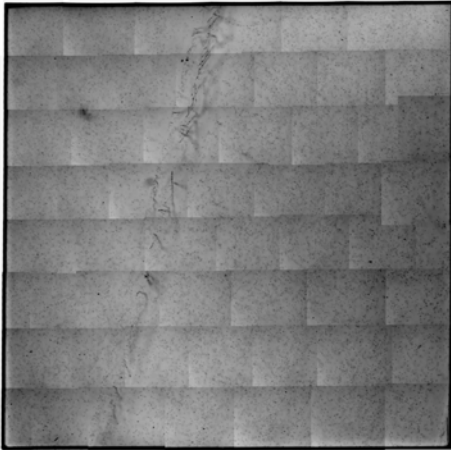


Figure 7. Infrared transmission image of first specimen evaluated with the 2 mm pixel configuration.

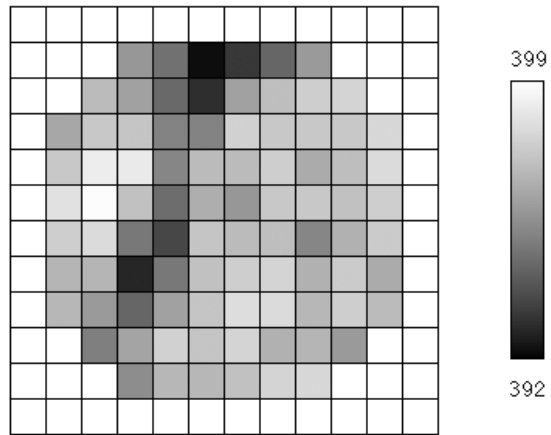


Figure 8. Pixel map showing the peak channel position for the  $\text{Am}^{241}$  59.6 keV line. This pixel map has the same orientation as the infrared transmission image shown in Figure 7.

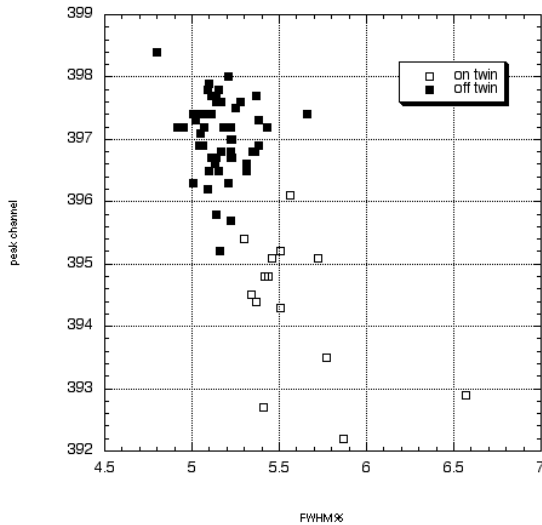


Figure 9. Scatter plot of peak channel position versus FWHM for pixels on and off the twinned region in the first specimen evaluated with 2 mm pixels.

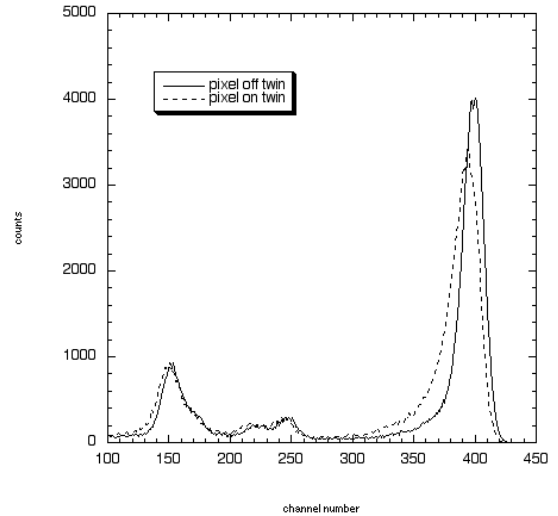


Figure 10.  $\text{Am}^{241}$  spectra from the most efficient pixel off the twinned region and the least efficient pixel on the twinned region. The peak at channel 150 is the silver K-alpha line fluoresced from the CHO-SEAL 1224. The lower energy  $\text{Am}^{241}$  lines are attenuated by the CHO-SEAL 1224.

The second specimen evaluated also contains three twin planes, however one of these planes is confined to the edge of the specimen and hence was not evaluated (recall that the 44 edge pixels were not evaluated). The twin region that was evaluated consists of two parallel twin planes. A schematic drawing of the twin planes is shown in Figure 11 and an infrared transmission image of the specimen is shown in Figure 12.

The map of the peak channel position for this specimen, which is Figure 13, shows no correlation with the twin planes (the map and the infrared transmission image in Figure 12 are in the same orientation).

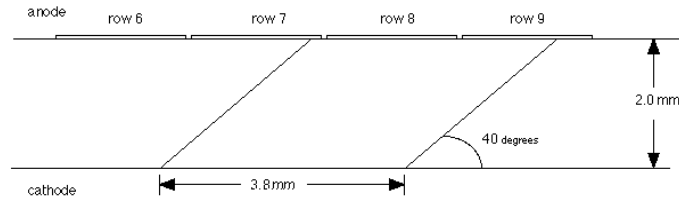


Figure 11. Schematic drawing of the two twin planes evaluated in the second specimen with 2 mm pixels.

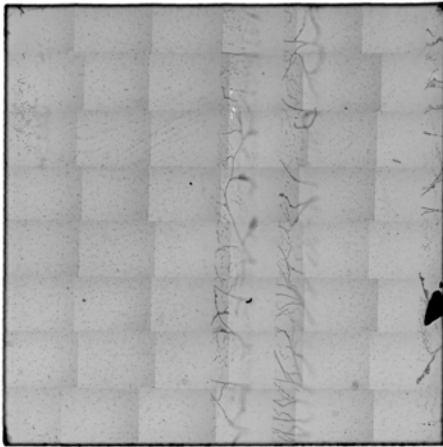


Figure 12. Infrared transmission image of second specimen evaluated with 2 mm pixels. Note that the twin on the right specimen edge was not evaluated.

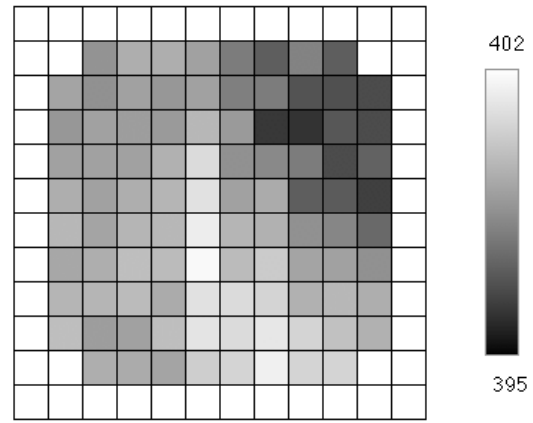


Figure 13. Pixel map showing peak channel position for the  $\text{Am}^{241}$  59.6 keV line. Note that there is no correlation between detector performance and the twin plane locations.

There are several factors which may explain this result. For the first specimen, the relatively small lateral separation between the three twin planes and the steep through-the-thickness twin plane angle creates a geometry where electrons moving in the electric field of a single 2mm pixel will encounter all three twin planes. For the second specimen, there is a much greater lateral separation between the twin planes, and as can be seen in Figure 12, the twin planes are not completely within the active volume of any pixels and there is no instance where charge carriers will encounter more than one twin plane. Not surprisingly, these findings suggest that the number of twin planes decorated with tellurium inclusions bisecting the active volume of a pixel will determine the extent of performance degradation. Our results show that isolated single twin planes may not produce a detectable difference in performance for 2mm pixel detectors. When multiple twin planes are present, the average downward shift in peak channel position for the  $\text{Am}^{241}$  59.6 keV line was 0.6 percent and the average increase in FWHM was 0.3 keV. The worst case for a 2 mm pixel was a 1.1 percent downward shift in peak position and a 0.9 keV increase in FWHM.

### 3.2 X-ray spectral mapping

During recent x-ray spectral mapping of 26.9 by 26.9 by 2 mm HPB CdZnTe specimens for the University of Arizona Department of Radiology, we discovered that our x-ray spectral mapping system was capable of detecting twin boundaries. The specimen in question contained 20 twin planes within a lateral spacing of 9.3 mm. The through-the-thickness angle of the twin planes was approximately 76 degrees. A schematic

of the twin plane configuration is shown in Figure 14 and an infrared transmission image of the specimen is shown in Figure 15. For spectral mapping, the specimen was configured with four large (approximately 12 by 12 mm) anode pixels and a planar cathode. We employed a 250 micrometer diameter collimator and a 250 micrometer step size. Maps of peak channel position (Figure 16) and counts in the peak channel (Figure 17) for the tungsten K-alpha line (59.3 keV) were created after performing a five point averaging algorithm to smooth the spectral data. These maps show that the twin boundaries produce a downward shift in peak channel position and an accompanying loss of efficiency. Note that not all of the twin boundaries are evident in the map. We were able to establish that the regions of poor performance correspond to those locations where there are two or three twin planes spaced within several hundred micrometers. At these tight spacings, the charge carries created within the 250 micrometer collimated spot will encounter multiple twin planes. This result, which is consistent with the results obtained from the 2 mm detectors, suggests that multiple tightly spaced twin planes are capable of producing detectable degradation in detector performance.

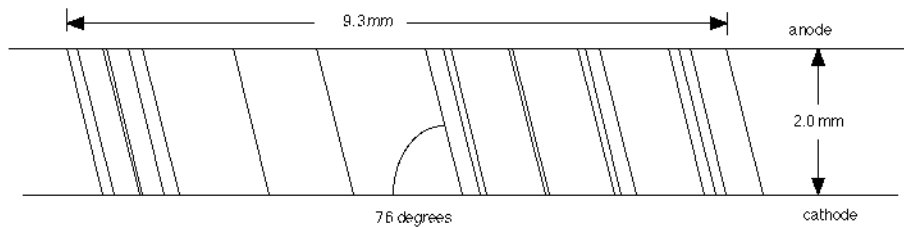


Figure 14. Schematic drawing of the 20 twin planes found in the specimen mapped for the University of Arizona.

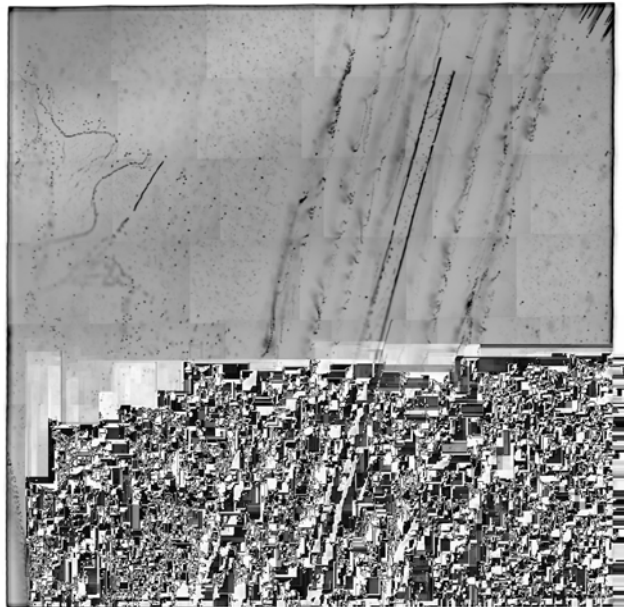


Figure 15. Infrared transmission image of the specimen mapped for the University of Arizona.

We also noted that the areas directly adjacent to the areas of poor performance appear to be slightly more efficient than the areas away from the twinned region. We are not certain if this is due to variations in the electric field created by the twin, i.e., a concentration of the field lines, or by the fact that these areas tend to have a significantly lower concentration of tellurium inclusions compared to the surrounding bulk

material. This effect can be seen most clearly in the infrared transmission images in Figures 12 and 15. Hence, these results do not clearly indicate if the twins channel or trap charge.

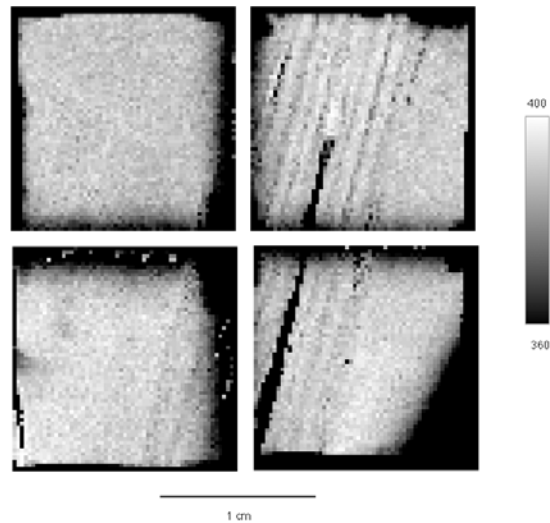


Figure 16. X-ray spectral map for 4 large anode pixels on the specimen shown in Figure 15. This map is the tungsten K-alpha line (59.3 keV) peak channel position and it shows that the twins again produce downward shifts in the peak channel position.

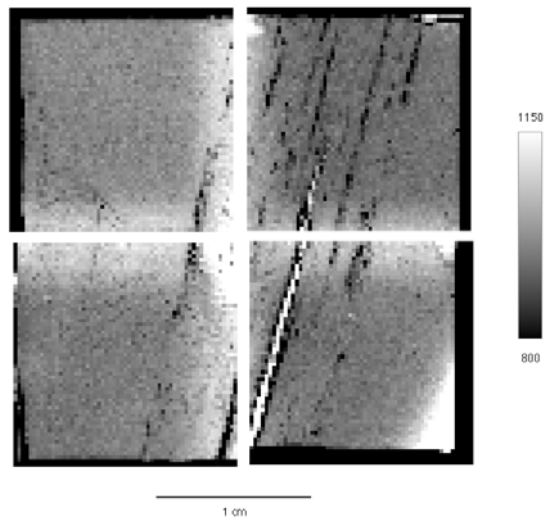


Figure 17. An additional spectral map for the specimen shown in Figure 15. This map is a plot of the counts in the peak channel. The map shows that for some twin regions, the downward peak shift is accompanied by a loss in efficiency.

In order to compare results obtained in the 2 mm pixel configuration with results from the x-ray spectral mapping system, we converted the first 26.9 by 26.9 by 2 mm specimen (Figures 6, 7 and 8) into a four pixel large anode detector by electrically interconnecting groups of 36 pixels. We mapped a portion of one of the large pixels intersected by the three twin planes using a 100 micrometer collimator and 100 micrometer step size. Maps of peak channel position and counts in the peak channel for the tungsten K-

alpha line at 59.3 keV are shown in Figures 18 and 19, respectively. Both of these maps were produced after performing a five point smoothing algorithm. The maps show that the area of poorer performance is confined to very narrow bands, i.e., the degradation is not uniform over the approximately 2.2 mm wide region defined by the three twin planes (see Figure 6). The band with the most significant loss of efficiency in Figure 19 appears to correspond to the narrow region within the material where electrons will encounter three twin planes. This finding, which needs to be substantiated with results from additional specimens, suggests that electron trapping is one degradation mechanism created by tellurium inclusions in HPB CdZnTe.

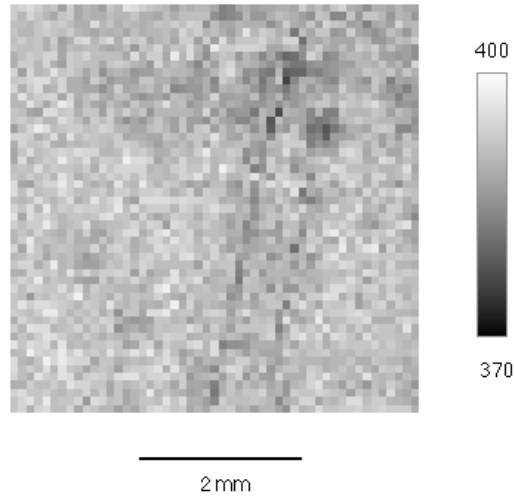


Figure 18. X-ray spectral map of the peak channel position of the tungsten K-alpha line (59.3 keV) for a portion of a 12.5 by 12.5 mm pixel on the specimen shown in Figure 7. The map shows the downward shift in peak channel position produced by the twin planes.

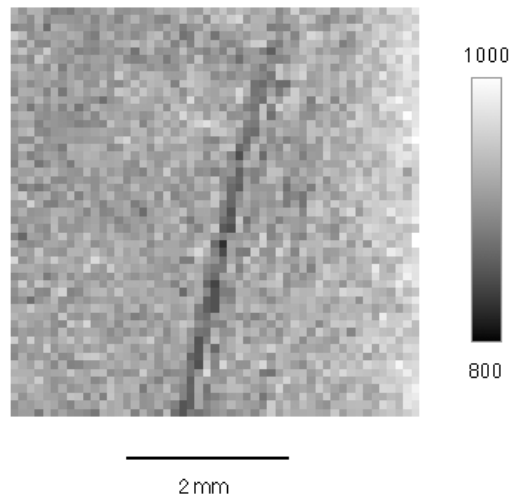


Figure 19. X-ray spectral map showing counts in the peak channel for the same area as shown in Figure 18.

## 4. CONCLUSIONS

When two or more twin planes bisect the active volume of a HPB CdZnTe detector pixel, there is detectable degradation in detector performance. The degradation takes the form of a downward shift in peak channel position accompanied by an increase in the peak FWHM. The extent of the degradation is dependent on the twin plane geometry and the detector configuration. The worst case for a 2 mm thick detector with 2 mm pixels and Am<sup>241</sup> flood illumination was an approximately 1.1 percent downward shift in peak channel position with a 0.9 keV increase in FWHM for the 59.6 keV line.

The results suggest that tellurium inclusions, which invariably decorate the twin planes, create the degradation. As the density of twin planes within the active volume of a pixel increases, the density of tellurium inclusions within the active volume also increases. The high concentration of tellurium inclusions on the twin planes creates areas directly adjacent to the twins with a lower than average concentration of dispersed tellurium inclusions. The fact that we often see better than average performance in these areas again suggests that the density of tellurium inclusions directly effects detector performance.

If possible, HPB material should be selected as single grain with no twins and a uniform distribution of dispersed tellurium inclusions. However, we suspect that the yield of large area twin free specimens would be extremely low. The yield can be improved by selecting material with twin planes that have geometries (lateral twin plane spacing and through-the-thickness angle) that prevent overlap of the planes in the thickness dimension. This twin geometry should create little variation in the density of tellurium inclusions for pixels 2 mm and larger. For smaller pixel devices, the string-like formations of tellurium inclusions often seen on twin planes may create detectable degradation, even in the most favorable geometry.

## ACKNOWLEDGEMENTS

Funding for this research was provided by the NASA Office of Safety and Mission Assurance. We also want to acknowledge eV Products, Inc. for the numerous specimens provided for study.

## REFERENCES

1. T. Narita, P.F. Bloser, J.E. Grindlay, J.A. Jenkins, "Development of Gold Contacted Flip-chip Detectors with IMARAD CZT," *Hard X-Ray, Gamma-Ray and Neutron Detector Physics II*, R. James and R. Schirato, eds., *Proc. SPIE* **4141**, p. 89, 2000.
2. T.H. Prettyman, M.C. Browne, K.D. Ianakiev, C.E. Moss, "Characterization of a large-volume, multi-element CdZnTe detector," *Hard X-Ray, Gamma-Ray and Neutron Detector Physics II*, R. James and R. Schirato, eds., *Proc. SPIE* **4141**, p. 1, 2000.
3. S.D. Barthelmy, "Burst alert telescope (BAT) on the Swift MIDEX mission," *X-ray and Gamma-ray Instrumentation for Astronomy XI*, K. Flanagan and O. Siegmund, eds., *Proc. SPIE* **4140**, 2000.
4. InFOC $\mu$ S web site: <http://infocus.gsfc.nasa.gov/detect.html>
5. P. Bloser, T. Narita, J. Jenkins, J. Grindlay, "Construction and Testing of Pixellated CZT Detector and Shield for a Hard X-ray Astronomy Balloon Flight," *X-ray and Gamma-ray Instrumentation for Astronomy XI*, K. Flanagan and O. Siegmund, eds., *Proc. SPIE* **4140**, 2000.
6. F. Harrison, S. Boggs, A. Bolotnikov, C. Chen, W. Cook S. Schindler, "Development of CdZnTe pixel detectors for astrophysical applications," *Hard X-Ray, Gamma-Ray and Neutron Detector Physics II*, R. James and R. Schirato, eds., *Proc. SPIE* **4141**, p. 137, 2000.

7. B. Parker, C. Stahle, S. Barthelmy, A. Parsons, J. Tueller, J. Van Sant, B. Munoz, S. Snodgrass, R. Mullinix, "Correlation between bulk material defects and spectroscopic response in cadmium zinc telluride detectors," *Hard X-Ray, Gamma-Ray and Neutron Detector Physics*, R James and R. Schirato, eds., *Proc. SPIE* **3768**, p. 129, 1999.
8. T.E. Schlesinger and R.B. James, *Semiconductors for Room Temperature Nuclear Detector Applications*, SEMICONDUCTORS AND SEMIMETALS, Vol 43, p. 268, Academic Press, 1995.
9. D. Roth, B. Parker, D. Rapchun, H. Jones, W. Cao, *LabVIEW Interface Concepts Used in NASA Scientific Investigations and Virtual Instruments*, NASA/TM-2001-210683, 2001.